Supporting Information

Harnessing Zinc(II) bis-Terpyridine Complex to Overcome Drug Resistance: Mechanistic Insights for Antibacterial Activity

Sourav Sutradhar,[a§] Saurabh Gupta,[b§] Parnashabari Sarkar,[a] Dipankar Das,[a] Kamaldeep Paul,[*b,c] Biswa Nath Ghosh*[a]

[a]*Department of Chemistry, National Institute of Technology Silchar, Silchar, Assam, India.* bnghosh@che.nits.ac.in

[b]*TIET-VT, Centre of Excellence in Emerging Materials, Thapar Institute of Engineering and Technology, Patiala, Punjab, India-147004*

[c]*Department of Chemistry and Biochemistry, Thapar Institute of Engineering and Technology, Thapar, Punjab, India.* kpaul@thapar.edu

§ Equally contributed

Figure S1	400 MHz ^{1}H NMR spectrum of ligand **L** in $CDCl_3$	**5**
Figure S2	100 MHz ^{13}C NMR spectrum of ligand **L** in $CDCl_3$	**5**
Figure S3	400 MHz ^{1}H NMR spectrum of Zn**L**$_2$ in DMSO-d_6	**6**
Figure S4	^{1}H NMR spectra of Zn**L**$_2$	**6**
Figure S5	HRMS spectrum of Zn**L**$_2$	**7**
Figure S6	UV-visible absorption spectrum of Zn**L**$_2$ in acetonitrile	**7**
Figure S7	FTIR spectra of Zn**L**$_2$	**8**
Figure S8	UV-Visible absorption spectra of Zn**L**$_2$ at different time intervals in PB buffer at pH 7.4.	**8**
Table S1	Antibacterial activity of zinc complex	**9**
Table S2	Crystallographic data and structural refinement parameter for the Zn**L**$_2$	**11**
Table S3	Selected bond lengths (Å) and bond angles (°) of Zn**L**$_2$ complex	**11**
Figure S9	(a) Inhibition of biofilm; (b) auto-aggregation; (c) inhibition of surface hydrophobicity; and (d) loss in EPS content of *B. subtilis* and *S. enterica* in the presence of Colistin . *P <0.05; **P < 0.01; ***P < 0.001. n = 3	**18**
Figure S10	(a) Membrane depolarisation, (b) outer membrane permeability and (c) inner membrane permeability of *B. subtilis* and *S. enterica* by Colistin *P <0.05; **P < 0.01; ***P < 0.001. n = 3	**18**
Figure S11	(a) Loss in metabolic activity; (b) intracellular ROS production; (c) loss in GSH activity and (d) malondialdehyde production in *B. subtilis* and *S. enterica* treated with colistin. *P <0.05; **P < 0.01; ***P < 0.001. n = 3	**19**
Figure S12	Absorption spectra of **L** with increasing concentrations of ct-DNA in HEPES buffer (pH 7.4)	**19**
Figure S13	Benesi-Hildenbrand plot $A_0/(A - A_0)$ vs 1/[DNA] of UV-visible absorption spectra of **L** in the presence of ct-DNA in HEPES buffer (pH 7.4).	**20**
Figure S14	Benesi-Hildenbrand plot $A_0/(A - A_0)$ vs 1/[DNA] of UV-visible absorption spectra of Zn**L**$_2$ in the presence of ct-DNA in HEPES buffer (pH 7.4)	**20**
Figure S15	Stern-Volmer plot {I_0/I vs. [Zn**L**$_2$]} of emission spectra of DNA in the absence and presence of Zn**L**$_2$	**21**
Figure S16	Absorption spectra of HSA with increasing concentration of **L** at 298 K in PBS buffer (pH 7.4).	**21**
Figure S17	Benesi-Hildebrand plot {$A_o/(A-A_o)$ vs. 1/ **[L]**} of absorption spectra of	**22**

	HSA in the absence and presence of **L** in PBS buffer at 298 K.	
Figure S18	Benesi-Hildebrand plot {$A_o/(A-A_o)$ vs. 1/ **[**ZnL_2**]**} of absorption spectra of HSA in the absence and presence of ZnL_2 in PBS buffer at 298 K	**22**
Figure S19	Emission spectra of HSA with increasing concentration of **L** at 298 K in PBS buffer (pH 7.4)	**23**
Figure S20	Stern-Volmer plot {F_0/F vs. [**L**]} of emission spectra of HSA in the absence and presence of **L** in PBS buffer at 298 K.	**23**
Figure S21	Modified Stern-Volmer plot of emission spectra of HSA in the absence and presence of **L** in PBS buffer at 298K	**24**
Figure S22	Stern-Volmer plot {F_0/F vs. [ZnL_2]} of emission spectra of HSA in the absence and presence of ZnL_2 in PBS buffer at 298 K	**24**
Figure S23	Modified Stern-Volmer plot of emission spectra of HSA in the absence and presence of ZnL_2 at 298 K	**25**
Figure S24	Modified Stern-Volmer plots of fluorescence spectrometer titration of warfarin-HSA complex with ZnL_2	**25**
Figure S25	Modified Stern-Volmer plots of fluorescence spectrometer titration of ibuprofen-HSA complex with ZnL_2	**26**
Figure S12	Time decay profile of HSA on gradual addition of ZnL_2 in PBS buffer (*p*H 7.4)	**26**

Synthesis of ligand L

The ligand **L** was synthesized according to the literature method[S1] where, 2-acetylpyridine (2.42 mL, 20mmol) was taken in a double-neck round bottle flask. A methanolic solution of 3,4-diethoxybenazaldehyde (1.77 mL, 10 mmol) and KOH (1.3 g, 20 mmol) was added to the round bottle flask. After the ammonia (30mL) the solution was kept for stirring at room temperature for 8 hours. The crude product was washed with distilled water and methanol. The product was dissolved in a minimum amount of chloroform (8 mL) and recrystallized with excess *n*-hexane to get off-white precipitates. The final product was purified through column chromatography using 3% methanol in chloroform. Yield 1.38g (6.9 mmol, 34%). ^{1}H NMR (400 MHz, $CDCl_3$) *δ*/ppm 8.73-8.71 (2H, m), 8.66-8.65 (4H, m), 7.89-7.85 (2H, m), 7.48 (1H, d), 7.40 (1H, d), 7.35-7.34 (2H, d), 6.99 (1H, d), 4.24 (2H, q), 4.18 (2H, q), 1.52-1.48 (6H, dt). ^{13}C NMR (100 MHz, $CDCl_3$) *δ*/ppm 156.5, 155.9, 150.3, 149.9, 149.2, 149.0, 137.0, 131.3, 123.9, 121.5, 120.4, 118.6, 113.3, 112.6, 65.0, 64.6, 14.9. FT-IR (υ_{max}/cm^{-1}): 3047 (aromatic sp^2-C-H str), 2977 (sp^3-C-H asym str of –CH_3), 2936 (sp^3-C-H asym str of –CH_2), 2874 (sp^3-C-H sym str of –CH_3), 1601, 1516, 1473, 1434 (aromatic C = C, C = N str), 1378, 1246 (aromatic C-O asym str), 1195, 1143 (aliphatic C-O str), 1042 (aromatic C-O sym str), 850 (C-H bending, *p*-sub), 795 (C-H bending, *m*-sub), 690 (C-H bending, *m*-sub), 614.

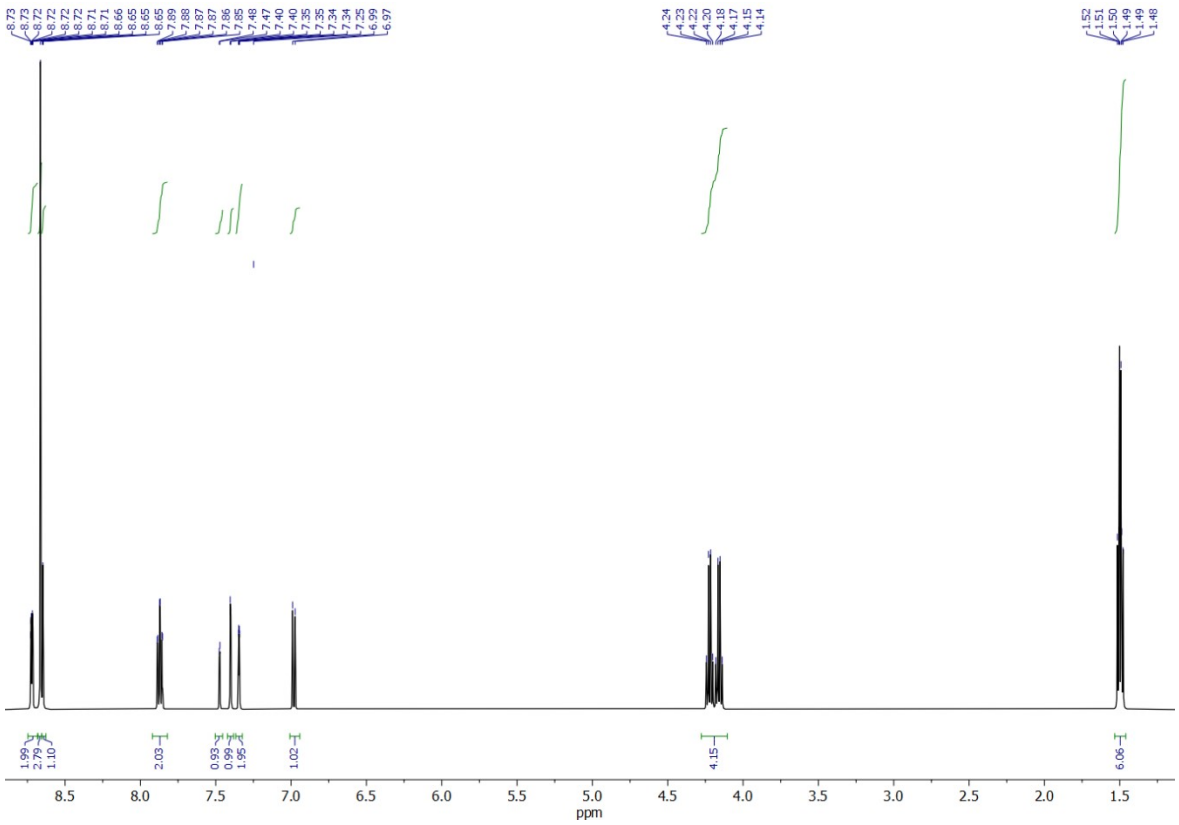

Figure S1: 400 MHz ^{1}H NMR spectrum of ligand **L** in $CDCl_3$.

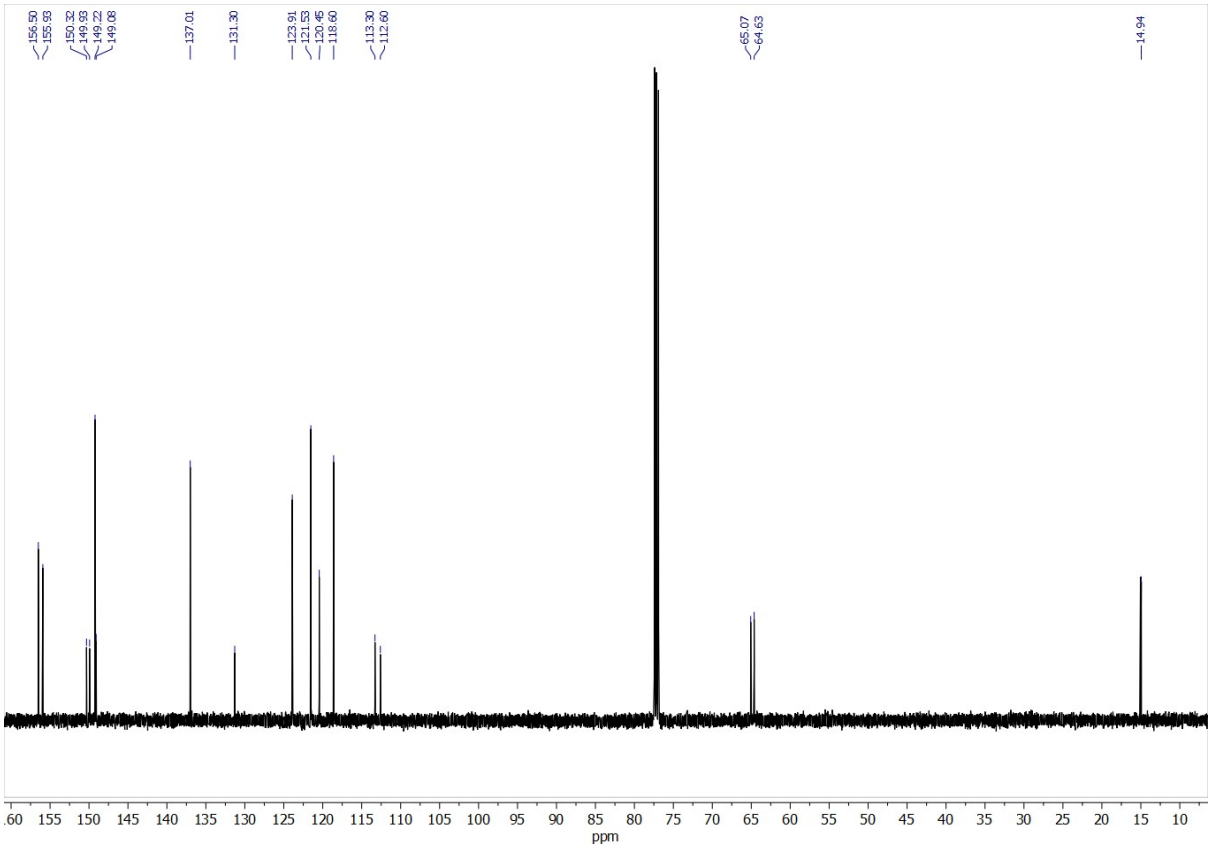

Figure S2: 100 MHz ^{13}C NMR spectrum of ligand **L** in $CDCl_3$.

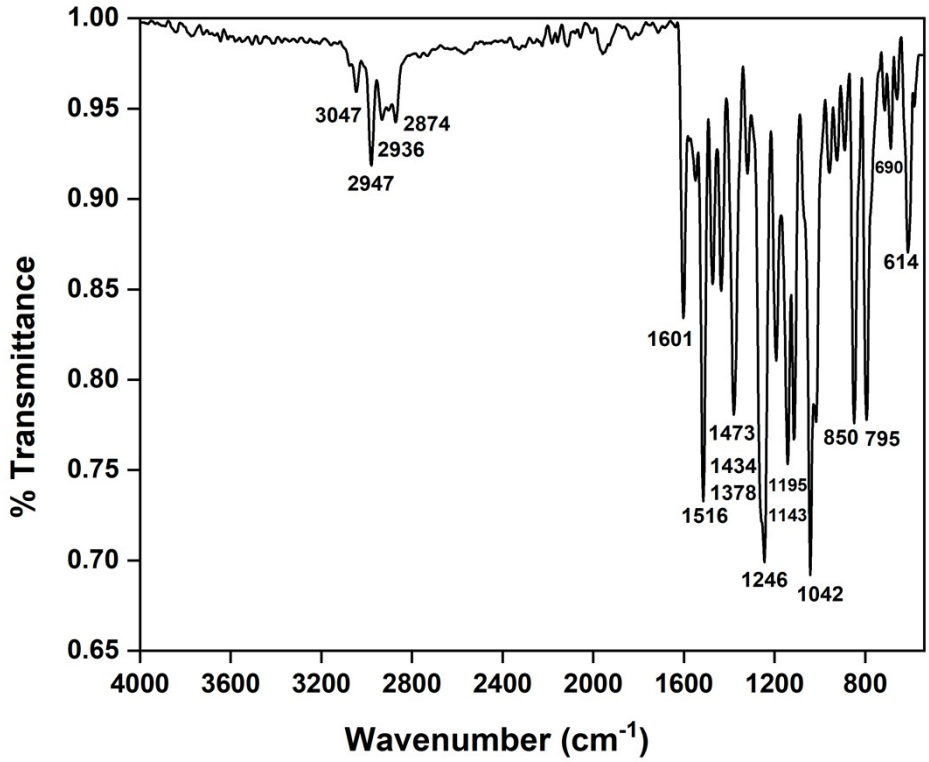

Figure S3: FTIR spectrum of ligand **L**

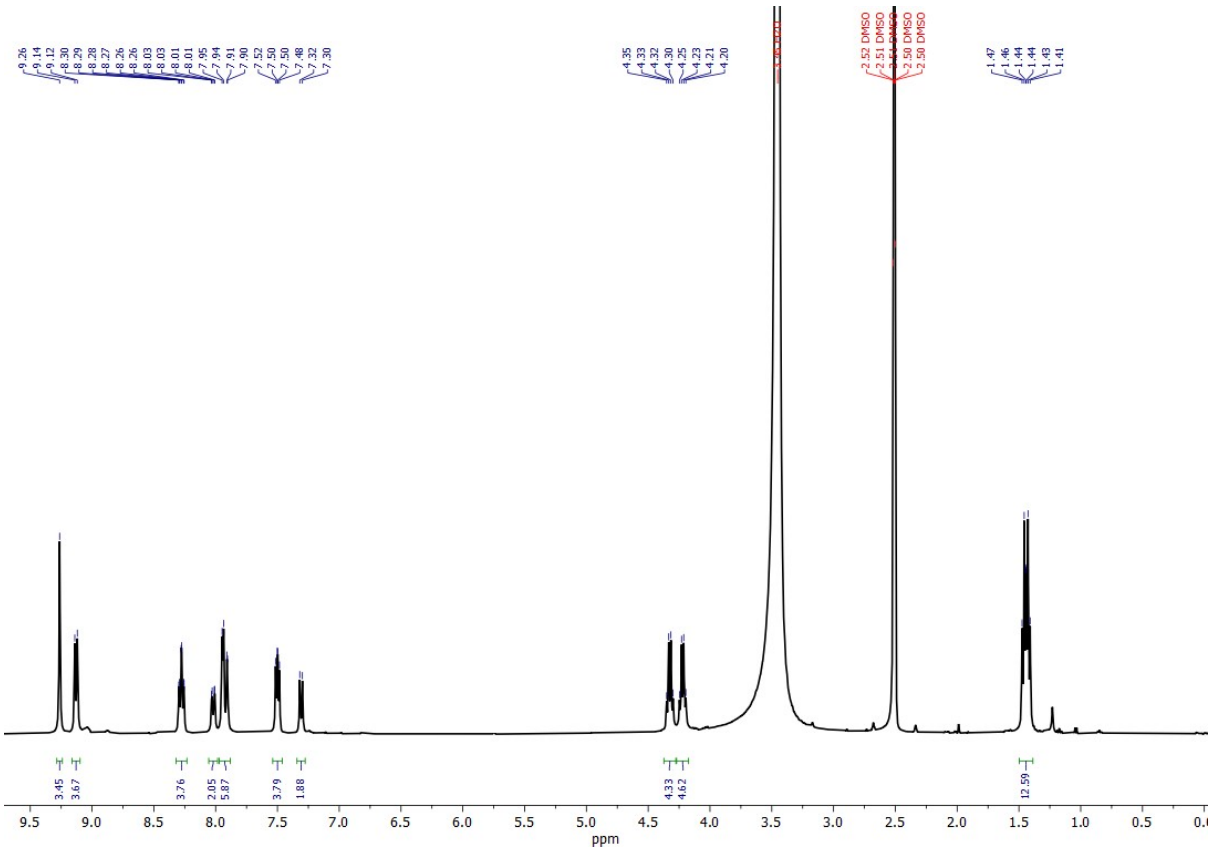

Figure S4: 400 MHz ^{1}H NMR spectrum of Zn**L**$_2$ in DMSO-d_6.

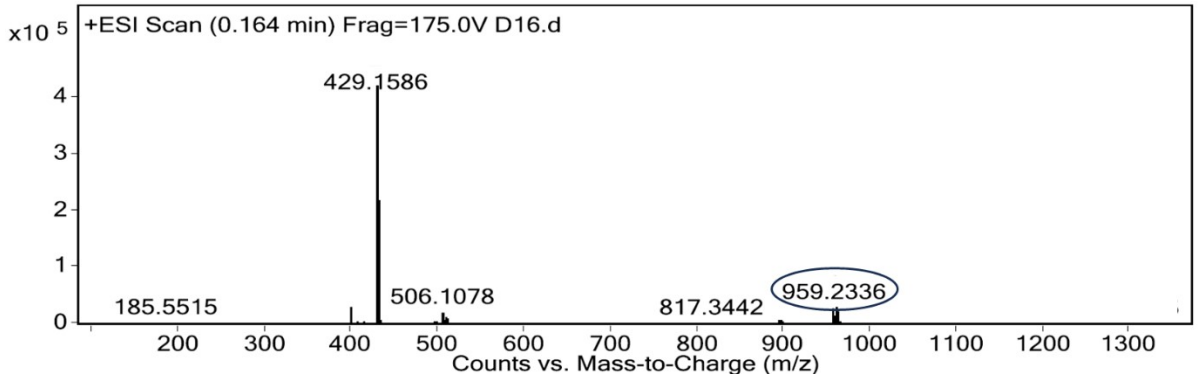

Figure S5: HRMS spectrum of Zn**L**$_2$.

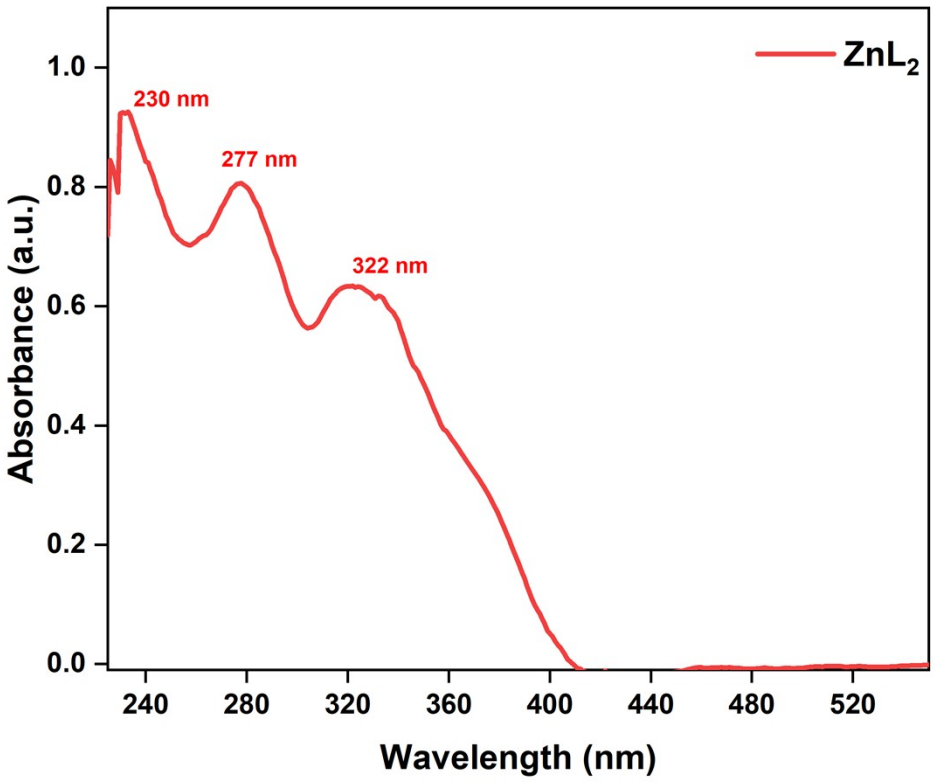

Figure S6: UV-visible absorption spectrum of Zn$\mathbf{L}_2$ in acetonitrile.

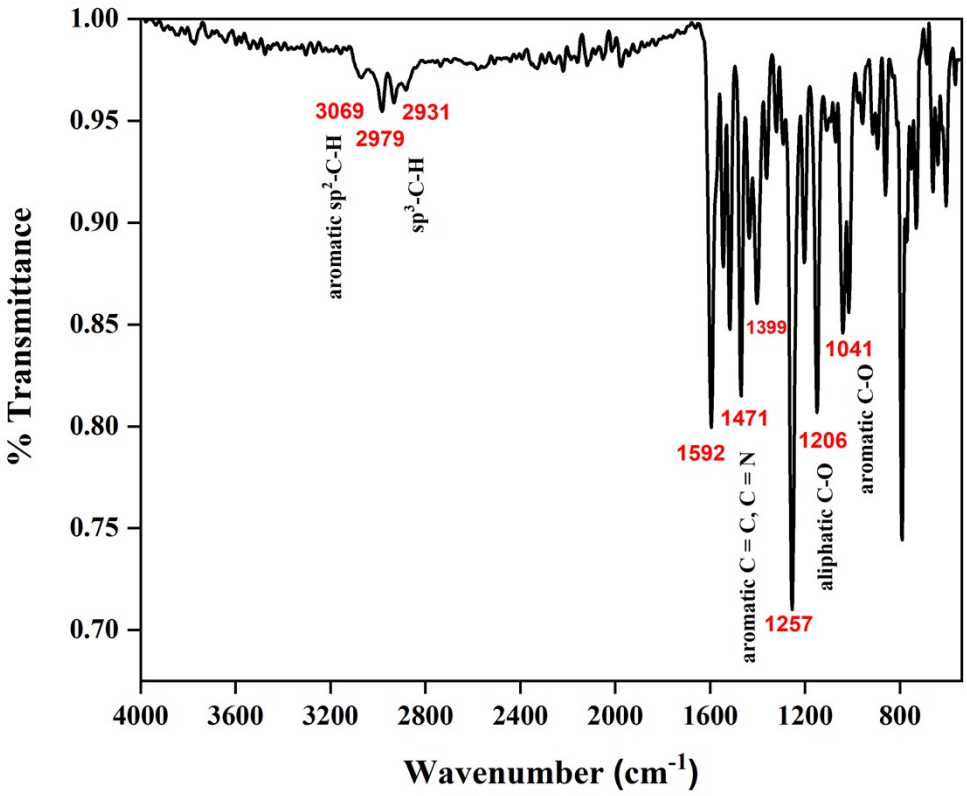

Figure S7: FTIR spectrum of Zn$\mathbf{L}_2$

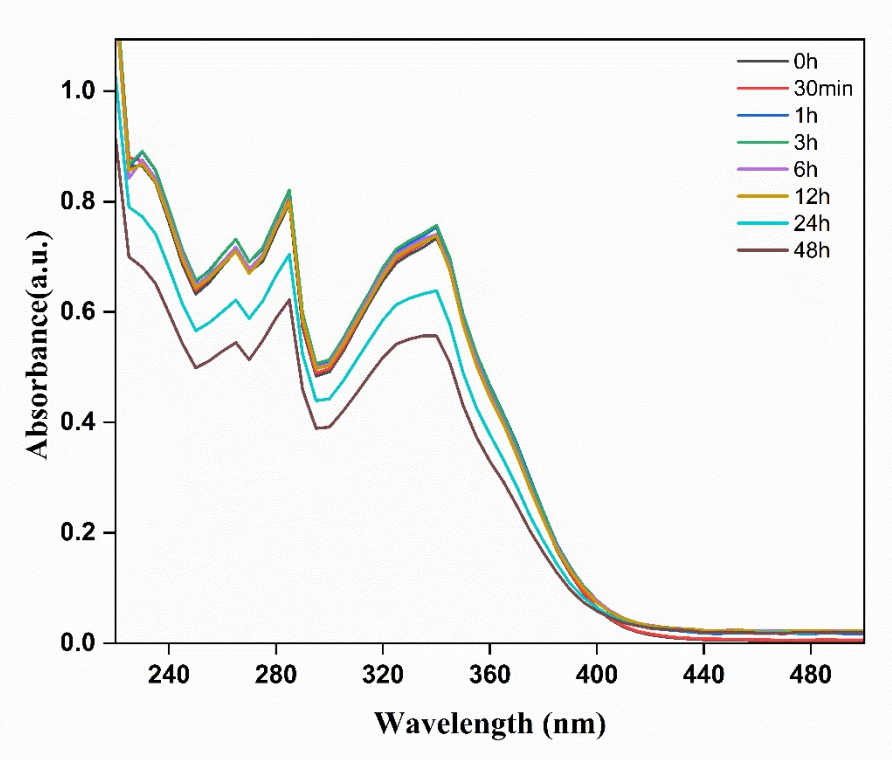

Figure S8: UV-Visible absorption spectra of Zn$\mathbf{L}_2$ at different time intervals in PB buffer at pH 7.4.

Table S1 Antibacterial activity of zinc complex

Zinc Complexes	Sensitive Bacterial Strain	MIC(μg/mL)	References
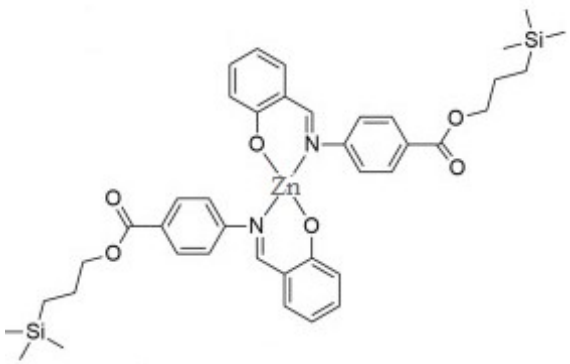	*Bacillus sp.* *Pseudomonas sp.*	32 0.50	S2
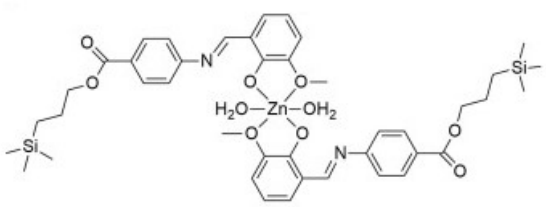	*Bacillus sp.* *Pseudomonas sp.*	32 0.50	S2
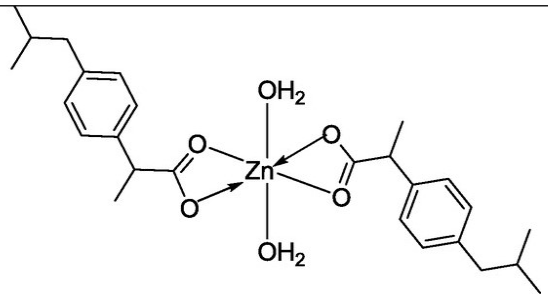	*B. subtilis* *S. aureus*	10.3 12	S3
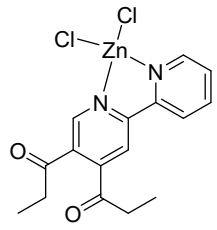	*P. aeruginosa* *S. aureus*	>500 500	S4
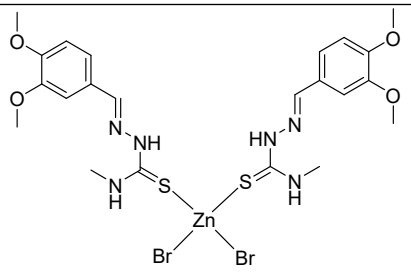	*B. subtilis* *E. faecalis*	>250 3.75	S5

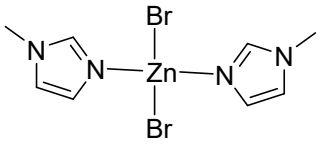	*E. coli* *S. aureus*	0.8 2.1	S6
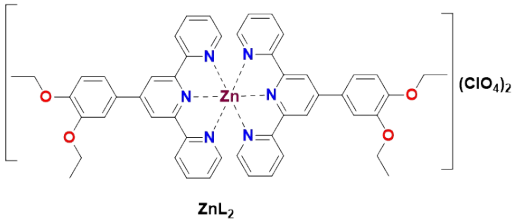	*B. subtilis* *S. enterica*	1.56 1.56	This Work

Single crystal diffraction studies

Yellow-coloured single crystals of **$[ZnL_2](ClO_4)_2.CH_3CN.H_2O$** were obtained by slow diffusion of di-isopropyl ether into an acetonitrile-methanol (1:1) solution of the zinc complex. Single Crystal X-ray diffraction data for the crystal was collected on a Bruker D8 VENTURE instrument. The diffractometer is equipped with a MoKα X-ray source with the wavelength 0.71073 Å. The program APEX4/SAINT (Bruker, 2021) [S7] was used to integrate the frames. A multi-scan absorption correction was done using the program SADABS (Bruker, 2016). [S8] The structure was solved by SHELXT 2018/2 (Sheldrick, 2018)[S9] and refined by full-matrix least-squares techniques using SHELXL-2019/2 (Sheldrick, 2019)[S10] computer program. All the hydrogen atoms were calculated to their optimal positions and treated as riding atoms using isotropic displacement parameters of either 1.2 or 1.5 larger than the corresponding carrier atoms. X-ray crystallographic data and structural refinement parameters for the complex are reported in Table S2. The R(int) is high due to weak diffraction data obtained from the crystal, especially at higher angles. There is a disorder observed in the solvent molecule (H_2O, and ACN) and the two perchlorate anions. The figure was drawn using the program *Mercury 2023.3.0*.[S11] Crystallographic data (excluding structure factors) for the structures in this paper have been deposited with the Cambridge Crystallographic Data Centre, CCDC, 12 Union Road, Cambridge CB21EZ, UK. Copies of the data can be obtained free of charge on quoting the depository numbers CCDC 2424188 (Fax: +44-1223-336-033; E-Mail: deposit@ccdc.cam.ac.uk, http://www.ccdc.cam.ac.uk).

Table S2: Crystallographic data and structural refinement parameter for the ZnL_2

Complex	**$[ZnL_2](ClO_4)_2.H_2O.CH_3CN$**
CCDC No	2424188

Empirical Formula	$C_{50}H_{46}N_6O_4Zn.Cl_2O_8.CH_3CN.H_2O$
M_w /g	1110.27
T /K	298(2) K
λ /Å	0.71073
Crystal system, space group	Monoclinic, P 21/n
a /Å	14.8069(13)
b /Å	18.8131(17)
c /Å	19.1316(17)
α /°	90
β /°	106.221(3)
γ /°	90
V /Å^3	5117.2(8)
Z	2
ρ_c /Mg/m^3	1.441
μ /mm^{-1}	0.656
F(000)	2304
Crystal size /mm	0.152 x 0.072 x 0.066
Theta range for data collection /°	2.523 to 25.081
Limiting indices	-17≤h≤17, -22≤k≤22, -22≤l≤22
Reflection collected	177558
Independent reflections	9069 [R(int) = 0.2498]
Completeness to θ_{full}	99.6%
Max. and min. transmission	0.7398 and 0.6337
Refinement method	Full-matrix least-squares on F^2
Data/restraints/parameters	9069 / 51 / 687
Goodness-of-fit on F^2	1.080
Final R indices[$I>2\sigma(I)$]	R1 = 0.0929, wR2 = 0.2077
R indices (all data)	R1 = 0.1465, wR2 = 0.2400
Largest diff. peak and hole/e·$Å^{-3}$	0.754 and -0.590

Table S3 Selected bond lengths (Å) and bond angles (°) of Zn**L**$_2$ complex.

Zn(1)-N(2)	2.069(5)	N(5)-Zn(1)-N(6)	75.25(19)
Zn(1)-N(5)	2.082(5)	N(1)-Zn(1)-N(6)	89.9(2)
Zn(1)-N(1)	2.161(5)	N(4)-Zn(1)-N(6)	149.87(19)
Zn(1)-N(4)	2.190(5)	N(2)-Zn(1)-N(3)	75.2(2)
Zn(1)-N(6)	2.201(5)	N(5)-Zn(1)-N(3)	96.6(2)
Zn(1)-N(3)	2.204(5)	N(1)-Zn(1)-N(3)	151.17(19)
N(2)-Zn(1)-N(5)	171.8(2)	N(4)-Zn(1)-N(3)	93.7(2)
N(2)-Zn(1)-N(1)	76.1(2)	N(6)-Zn(1)-N(3)	95.6(2)
N(5)-Zn(1)-N(1)	112.12(19)	C(11)-O(1)-C(22)	118.7(6)
N(2)-Zn(1)-N(4)	105.4(2)	C(12)-O(2)-C(24)	117.6(6)
N(5)-Zn(1)-N(4)	75.26(19)	C(36)-O(3)-C(47)	119.6(6)
N(1)-Zn(1)-N(4)	95.5(2)	C(37)-O(4)-C(49)	117.1(7)
N(2)-Zn(1)-N(6)	104.65(19)		

Biological assays

Minimal inhibitory concentration (MIC, μg/mL) is defined as the lowest concentration of target compounds that ultimately inhibit the growth of bacteria, using a standard two-fold serial dilution method in 96-well micro test plates according to the National Committee for Clinical Laboratory Standards (NCCLS). The tested bacterial strains were purchased from the Institute of Microbial Technology (IMTech), Chandigarh. Tetracycline, amoxicillin and chloromycin were used as control drugs. DMSO was inoculated with bacteria having no medicine as a positive control to check the effect of solvent bacterial growth. All the bacteria growths were monitored visually and spectrophotometrically, and the experiments were performed in triplicate.

Antibacterial assays

The synthesized ligand **L** and zinc complexes of **L** (1:1 and 1:2) were examined for their antibacterial activities against four gram-positive bacteria *viz* (*Staphylococcus aureus (*MTCC No-902)*, Enterococcus faecalis* (MTCC No-6845)*, Bacillus subtilis* (MTCC No- 441)*, Listeria* (MTCC No- 4214) and four gram-negative bacteria such as *Escherichia coli* (MTCC No-448)*, Salmonella enterica* (MTCC No-1165)*, Acinetobacter calcoaceticus* (MTCC No-1948)*, Serratia marcescens* (MTCC No-2645). The bacterial suspension was adjusted with sterile saline to a concentration of 1×10^5 CFU/mL. The stock solutions were prepared by dissolving compounds in DMSO. The compounds and reference drugs were prepared in Nutrient broth by two-fold serial dilution to obtain the required concentrations of 800, 400, 200, 100, 50, 25, 12.5, 6.25, 3.125, 1.56 μg/mL. These dilutions were inoculated and incubated at 37 ºC for 24 h.

Minimal bactericidal concentrations (MBC) assays

The minimal bactericidal concentrations (MBC) were determined by broth microdilution assay for Zn$\mathbf{L}_2$ against *B. subtilis and S. enterica*. This complex was 2-fold serially diluted and incubated with *B. subtilis and S. enterica* in a 96-well plate according to procedure outlined for MIC determination. After 24 h incubation period, 50 μL of the suspension from the microwell plate was plated onto tryptic soy agar (TSA). The lowest concentration showing no visible growth on the scale was considered the MBC value.

Bacterial susceptibility evaluation

After determining the MIC values, multiple passaging was performed by transferring bacterial suspension grown at sub-MIC. After the growth of *B. subtilis* and *S. enterica,* new MIC values

were calculated towards each passage of the strain; tetracycline, amoxicillin and chloromycin were taken as controls. The experiment was continued for 50 days.

Cytotoxicity toward a normal cell line

Human embryonic kidney (Hek293) cells were cultured in DMEM with 10% FBS, 50 mM glutamine, 100 mg/mL streptomycin, and 100 U/mL penicillin. Cells were seeded in two 96 well plates at the density of 1×10^{-5} cells/well in DMEM media supplemented with 10% FBS cells. Cells were incubated at 37 °C in a 5% CO_2 incubator. Cells were treated with Zn**L**$_2$ at five concentrations (0.78, 1.56, 3.125, 6.25, 12.5 μg/mL) at 37 °C for 48 h. 10 μL of MTT (prepared in 1* PBS buffer) from 5 mg/mL stock was added in each well and incubated at 37 °C for 4 h in the dark. The formazan crystals were dissolved using 100 μL of DMSO. Further, the amount of formazan crystal formation was measured as the difference in absorbance by Bio-Tek ELISA plate reader at 570 nm reference wavelength. All experiments were independently performed at least three times. The relative cell toxicity (%) related to control wells containing culture medium without test material was calculated using the following formula (eq. 1)

$$\%\ Cell\ Toxicity = 100 - \frac{OD\ (compound\ treated\ wells)}{OD\ (untreated\ wells)} \times 100 \quad \text{.....(1)}$$

Kinetics of bactericidal activity against *B. subtilis* and *S. enterica*

B. subtilis and *S. enterica* cells were incubated with Zn**L**$_2$ at different concentrations (MIC, 2 x MIC, 4 x MIC, 8 x MIC) in a 96-well plate at 37 ^{o}C. The absorbance values of untreated and treated cells were recorded for 6 h at an interval of 30 min, using an Elisa plate reader (Biotek, Power-Wave XS2). The decrease in value of absorbance was noted.

Biofilm inhibition assay

The bacterial suspension of *B. subtilis* and *S. enterica* was incubated with Zn**L**$_2$ at different concentrations in a 96-well plate for 72 h at 37 ^{o}C. The culture supernatant was discarded, and the sediment was washed with phosphate buffer. Then the plate was incubated for 1h at 60 ^{o}C to fix the biofilm. After incubating for 1 h, crystal violet dye (0.1%) was added to the stain for 1 h at room temperature. The excess dye was discarded and then rinsed with distilled water. Finally, 33% acetic acid was used to elute the stained biofilm. The absorbance was noted at 600 nm in a microplate reader.

Auto-aggregation test

Bacterial cells (8 mL) from overnight-grown cell culture were added to the test tube containing 2 mL of LB medium with and without Zn**L**$_2$ **(**MIC, 2 x MIC, 4 x MIC, 8 x MIC). All the test

tubes containing samples were incubated for 24 h at 37 °C under stirring conditions. After proper incubation, the test tubes were taken out of the incubator and allowed to stand statically for 30 min to settle down the bacterial cells. The absorbance of the uppermost portion of respective bacterial suspension was measured at 600 nm using the microplate absorbance reader without any disruption of the settled cells at the bottom of the tubes. The experiment was performed in triplicate.

Determination of hydrophobicity index

B. subtilis and *S. enterica* strains (250 μL) were grown in the presence of Zn**L**$_2$ (250 μL) at the concentration of MIC, 2 x MIC, 4 x MIC, and 8 x MIC in a centrifuge tube to incubate at 37 °C for 24 h with 1% DMSO as a negative control. After incubation, the bacterial solution (100 μL) treated with different concentrations of compounds was removed to measure the OD value at 600 nm (ODA_0), and then toluene (400 μL) was added to these centrifuge tubes, the solution was shaken at high speed for 1 min and allowed to stand for 10-15 min. The OD at 600 nm of the aqueous phase (ODA) was evaluated by a microplate absorbance reader. The hydrophobicity index was calculated according to the following formula: $[(ODA_0-ODA)/ODA_0] \times 100\%$. The experiment was performed in triplicate.

Congo red assay

B. subtilis and *S. enterica* strains (500 μL) were grown in the presence of Zn**L**$_2$ (500 μL) at the concentration of MIC, 2 x MIC, 4 x MIC, 8 x MIC in centrifuge tube to incubate at 37 °C for 24 h with 1% DMSO as a negative control. After incubation, the spent media containing planktonic cells were carefully discarded, followed by washing twice with PBS. Consequently, attached biofilm was stained with 1% (w/v) congo red solution and kept in dark condition for 30 min at room temperature. Then the excess unbound dye was removed by washing with PBS for thrice. Finally, the bound dye to the biofilm matrix was dissolved in 500 μL DMSO. The % of EPS matrix content was evaluated by measuring the optical density (OD) at 490 nm using a microplate absorbance reader. The EPS content was calculated according to the following formula: [ODsample/ (ODcontrol)] × 100%. The experiment was performed in triplicate.

Membrane depolarization assay

B. subtilis and *S. enterica* cells in mid-log phase (the OD600 values of about 0.400) were washed with a buffer solution (5 mM HEPES buffer, 5 mM glucose, pH 7.2) and the depolarizing fluid (5 mM HEPES buffer, 5 mM glucose, 50 mM KCl) was used to balance the membrane potentials for 0.5 h, following the depolarizing fluid was removed, the strains were dispersed in the buffer, and incubated with of 3,3′-dipropylthiadicarbocyanine iodide (diSC35)

dye (0.4 μM, 300 μL) for 1 h at 37 ^{o}C. After incubation with dye, the stained cells were washed with PBS to remove the excess dyes and re-suspended in the same buffer to an OD_{600} value of 0.065. *E. coli* was treated with Zn**L**$_2$ at MIC, 2 x MIC, 4 x MIC and 8 x MIC with DMSO and Triton X-100 used as negative and positive controls. Fluorescence intensity was measured using a fluorescence spectrophotometer at an excitation wavelength of 622 nm and emission wavelength of 670 nm for 30 min (control group).

Outer membrane disruption

The grown culture of *B. subtilis* and *S. enterica* was harvested at 3500 rpm for 5 – 10 min, washed, and suspended in a mixture of 5 mM glucose and 5mM Hepes buffer (1:1) at pH 7.2 to give a value of 10^8 CFU/mL. 150 μL of this bacterial suspension was transferred to 96 well plates and 50 μL NPN dye (10 μM) was added to the well, and the plate was incubated for 1 h. Fluorescence intensity was measured using a fluorescence spectrophotometer at an excitation wavelength of 350 nm and emission wavelength of 420 nm for 30 min (control group). Further, Zn**L**$_2$ was added, and the intensity of fluorescence was noted at various concentrations (1, 2, 4, 8 × MIC) under same conditions. Dimethyl sulfoxide was used as a negative control, and experiments were repeated in triplicates.

Inner membrane disruption

The grown culture of *B. subtilis* and *S. enterica* was harvested at 3500 rpm for 5 – 10 min, washed, and suspended in a mixture of 5 mM glucose and 5 mM HEPES buffer (1:1) at pH 7.2 to give a value of 10^8 CFU/mL. 150 μL of this bacterial suspension was transferred to 96 well plates, and 50 µL (EtBr) dye (10 μM) was added to the well, and the plate was incubated for 30 min. Fluorescence intensity was measured using a fluorescence spectrophotometer at an excitation wavelength of 520 nm and emission wavelength of 610 nm for 30 min (control group). Further, Zn**L**$_2$ was added, and the fluorescence intensity was noted at various concentrations (1 x, 2 x, 4 x, 8 x MIC) under the same conditions. Dimethyl sulfoxide was used as a negative control, and the experiment was repeated in triplicates.

Leakage of intercellular protein

The grown culture of bacteria's *B. subtilis* and *S. enterica* was incubated with increasing concentrations of Zn**L**$_2$ (1 x, 2 x, 4 x, 8 x MIC) for 24 h. Then, the mixture was centrifuged at 3500 rpm for 10 min, and the supernatant was collected. The concentration of the leaked protein in the supernatant was determined by standard follin assay.

Determination of DNA content

B. subtilis and *S. enterica* cells were collected by centrifugation at 8000 rpm for 6 min and washed with PBS (0.1 mM, pH 7.2). Cell suspensions (100 μL) were incubated at 37 ^{o}C under agitation treated with Zn$\mathbf{L}_2$ at MIC, 2 x MIC, 4 x MIC, 8 x MIC, and DMSO was used as negative control. The amounts of DNA from the cytoplasm into supernatant were estimated by detection of absorbance at 260 nm. The experiment was performed in triplicate.

Metabolic activity

The bacterial culture of *B. subtilis* and *S. enterica* was treated with increasing concentrations of Zn$\mathbf{L}_2$ for 6 h at 37 ^{o}C. The untreated and treated cells were incubated with resazurin dye (50 μg/mL, 25 μl) for 1 h at 37 ^{o}C, and then the absorbance was measured at 570 nm on an Elisa plate reader. The average % reduction was used to determine the metabolic activity.

Reactive Oxygen Species (ROS) production

Intracellular ROS was measured using a standard 2,7-dichlorofluorescein diacetate (DCFH-DA) assay. Then, 10^6 CFU/mL of *B. subtilis* and *S. enterica* cells were treated with increasing concentrations of Zn$\mathbf{L}_2$ for 6 h at 37 °C. Following treatment, both control and treated cells were harvested and washed with PBS, followed by incubation with 100 μM DCFH-DA probe for 30 min in the dark at 37 °C. The fluorescence originating from the oxidative cleavage of DCFH-DA to DCF was measured with a fluorescence spectrophotometer with an excitation wavelength of 485 nm and an emission wavelength of 528 nm. The increase in intracellular ROS production in cells treated with Zn$\mathbf{L}_2$ compared to control cells was plotted.

Intracellular Glutathione (GSH) activity

The activity of intracellular GSH was determined using a standard Ellman's assay. *B. subtilis* and *S. enterica* suspensions (~10^5 CFU/mL) were treated with increasing concentrations of compounds for 6 h at 37 °C. Both control and treated cells were centrifuged at 5000 rpm for 5 min, washed with PBS, and lysed. The clear supernatant was collected. Then, the Tris-HCl (50 mM) and 5,5-dithiobis(2-nitrobenzoic acid) (DTNB) (100 mM) were added and incubated for 30 min in dark at 37 °C. The resulting solution was measured at 412 nm by spectrophotometry (eq 2).

$$\left(1 - \frac{\text{OD@412 nm of treated}}{\text{OD@412 nm of control}}\right) \times 100 \qquad (2)$$

Lipid peroxidation

Malondialdehyde (MDA) is a natural product of lipid oxidation in organisms. Some aliphatic acids are gradually decomposed into complex compounds after oxidation, including MDA. Therefore, the level of lipid oxidation can be detected by detecting the level of MDA. The *B.*

subtilis and *S. enterica* suspensions (~10^5 CFU/mL) were treated with increasing concentrations of Zn**L**$_2$ for 4 h at 37 °C. Under the dark condition, trichloroacetic acid (TCA) was added to stop the reaction and then 0.5% thiobarbituric acid was added. The mixture was heated at 80 °C for 0.5 h. After using an ice bath to cool the mixture, both control and treated cells were centrifuged at 5000 rpm for 5 min, and then collected the supernatant and tested by a microplate reader at 535 nm.

Scanning electron microscopy (SEM)

The bacteria's *B. subtilis* and *S. enterica* was centrifuged at 3500 rpm for 5 min, and the supernatant was discarded. The bacteria cell was washed with PBS and suspended with PBS. The bacterial suspension was incubated with Zn**L**$_2$ (2 × MIC) for 4 h at 37 °C and centrifuged at 3500 rpm for 5 min and then washed thrice with PBS. The cells were fixed with 2.5 % glutaraldehyde overnight at 4 °C and washed with PBS buffer and dehydrated with different concentrations of ethanol (45, 55, 65, 75, 95 and 100%). Then, the pellet was transferred to silicon chip and dried. The samples were coated with gold and visualized under a scanning electron microscope.

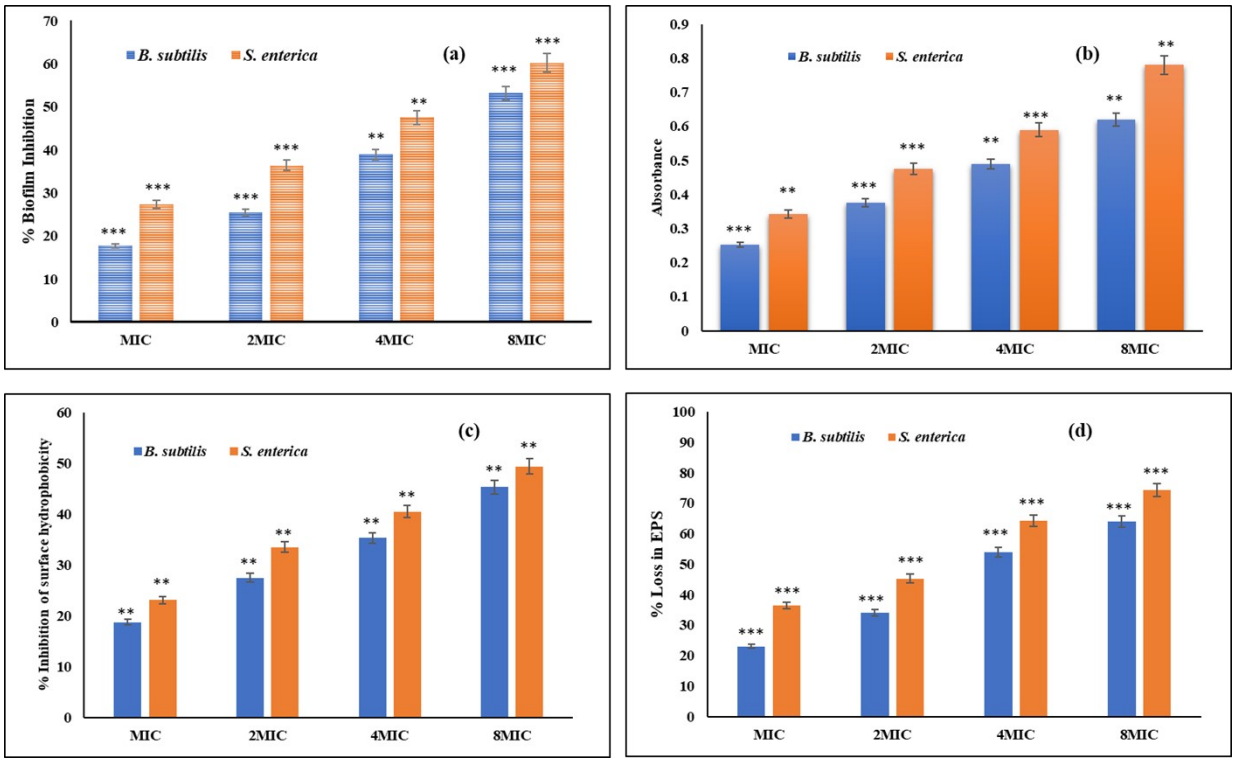

Figure S9: (a) Inhibition of biofilm; (b) auto-aggregation; (c) inhibition of surface hydrophobicity; and (d) loss in EPS content of *B. subtilis* and *S. enterica* in the presence of Colistin . *P <0.05; **P < 0.01; ***P < 0.001. n = 3

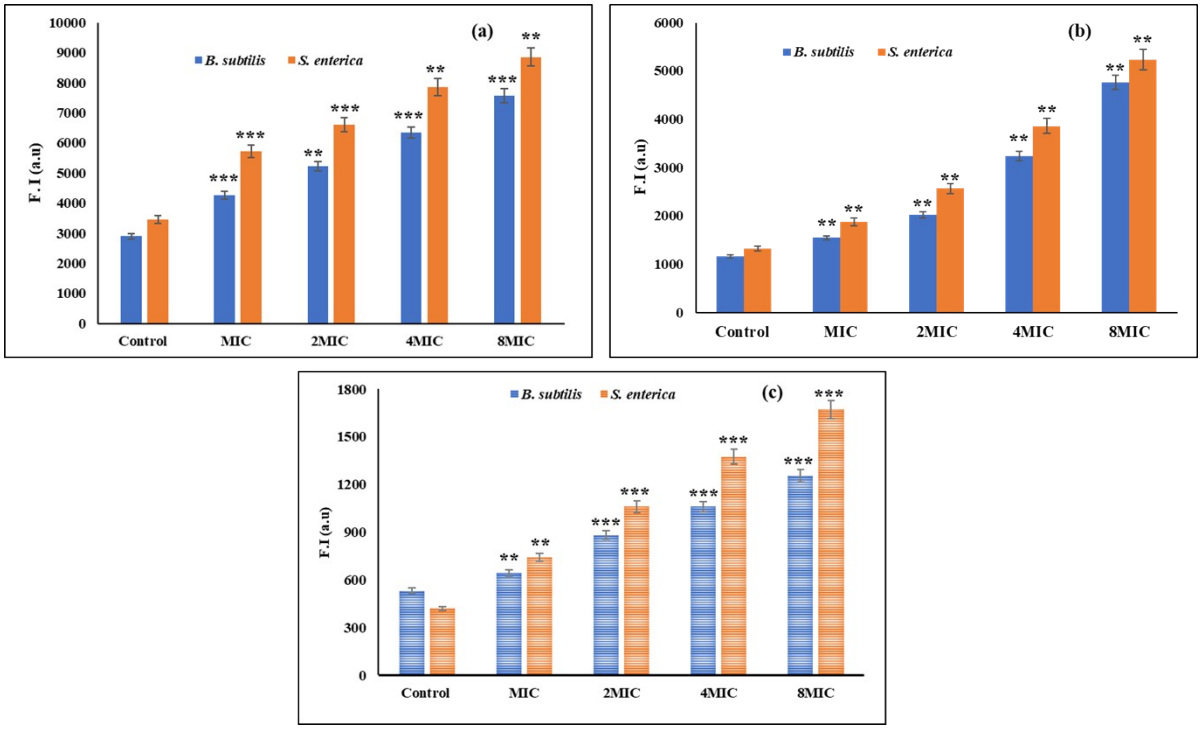

Figure S10: (a) Membrane depolarisation, (b) outer membrane permeability and (c) inner membrane permeability of *B. subtilis* and *S. enterica* by Colistin *P <0.05; **P < 0.01; ***P < 0.001. n = 3

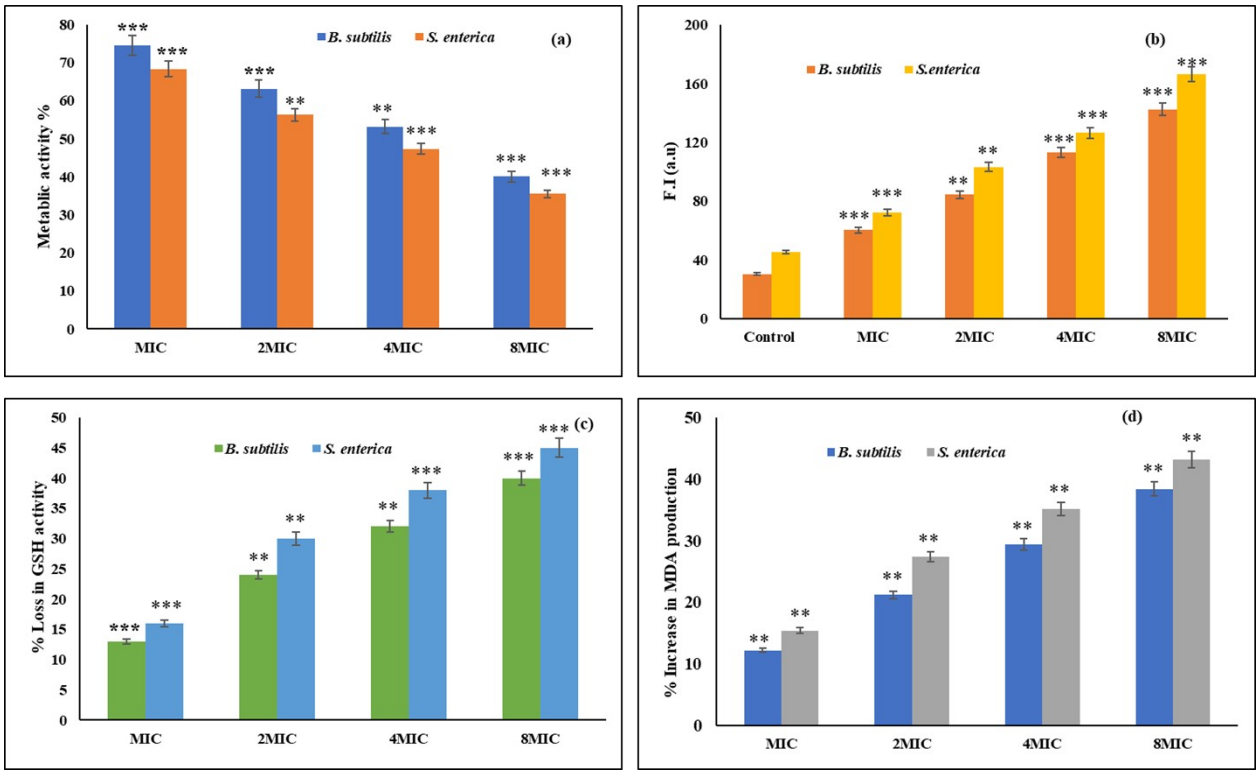

Figure S11: (a) Loss in metabolic activity; (b) intracellular ROS production; (c) loss in GSH activity and (d) malondialdehyde production in *B. subtilis* and *S. enterica* treated with colistin. *P <0.05; **P < 0.01; ***P < 0.001. n = 3

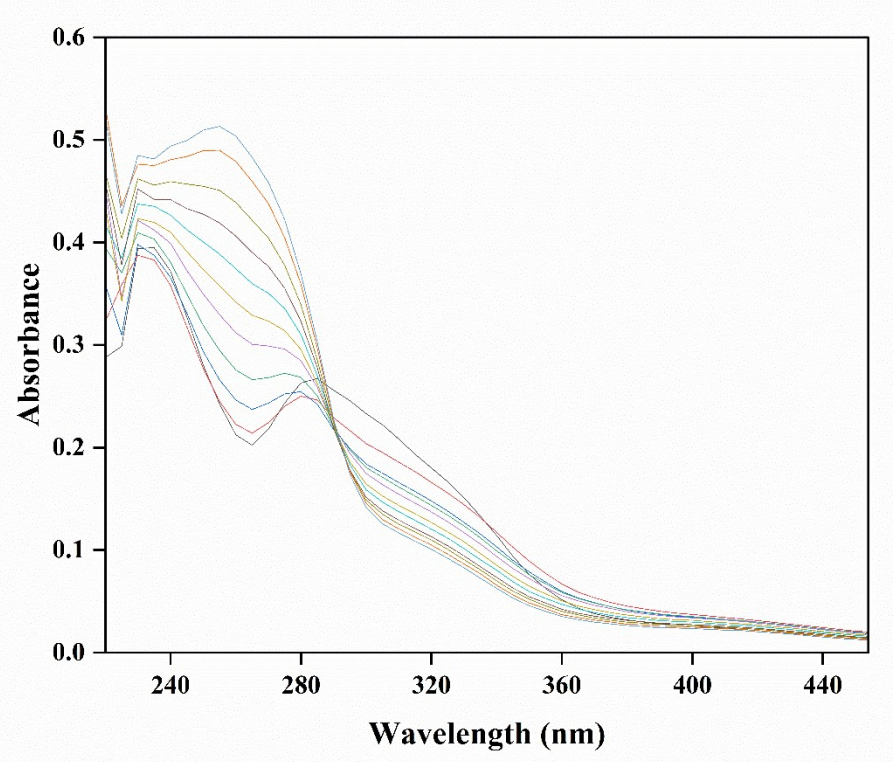

Figure S12: Absorption spectra of **L** with increasing concentrations of ct-DNA in HEPES buffer (pH 7.4)

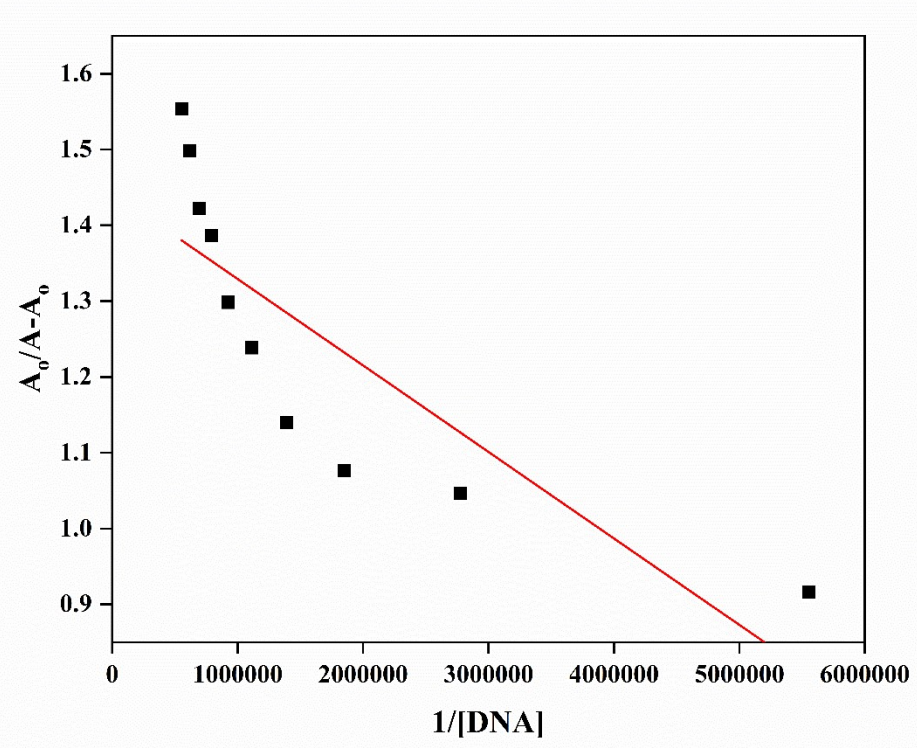

Figure S13: Benesi-Hildenbrand plot $A_0/(A - A_0)$ vs 1/[DNA] of UV-visible absorption spectra of **L** in the presence of ct-DNA in HEPES buffer (pH 7.4).

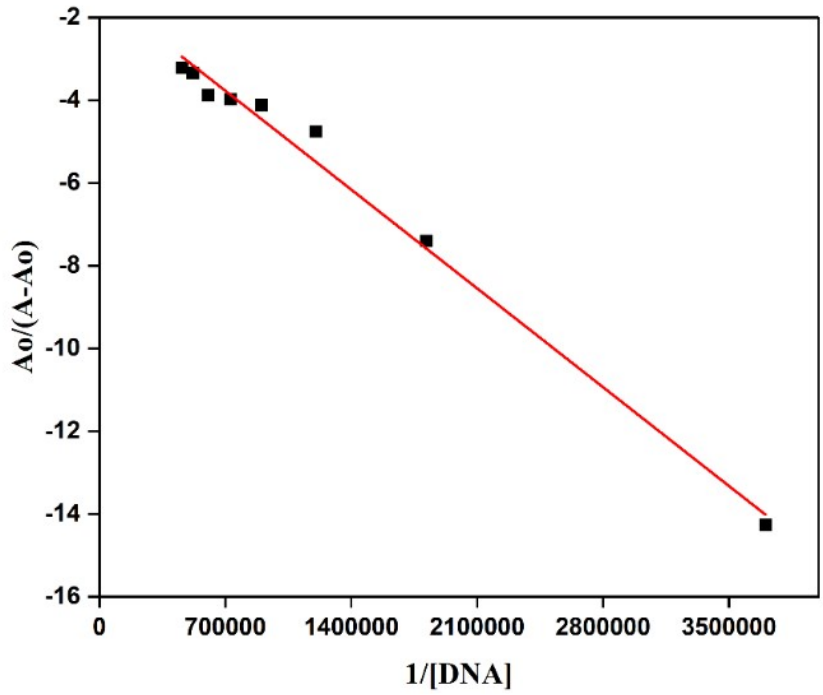

Figure S14: Benesi-Hildenbrand plot $A_0/(A - A_0)$ vs 1/[DNA] of UV-visible absorption spectra of Zn**L**$_2$ in the presence of ct-DNA in HEPES buffer (pH 7.4).

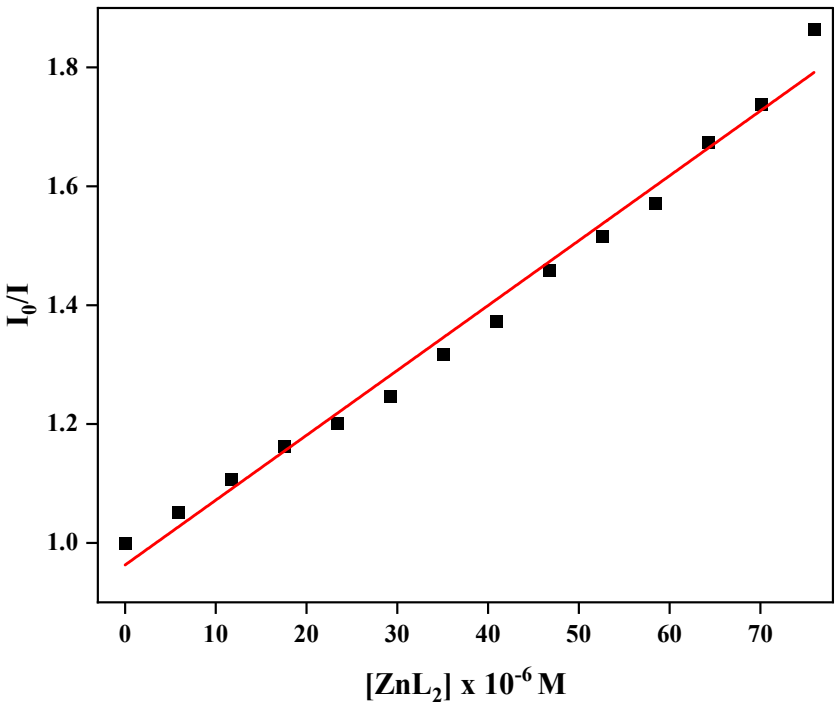

Figure S15: Stern-Volmer plot {I_0/I vs. [Zn**L**$_2$]} of emission spectra of DNA in the absence and presence of Zn**L**$_2$ in HEPES buffer (pH 7.4).

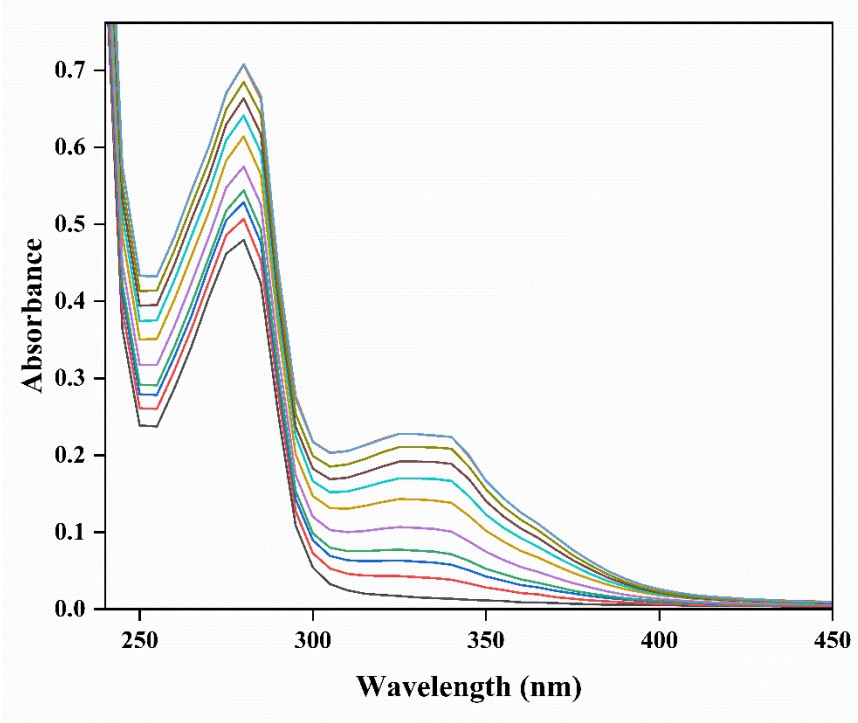

Figure S16: Absorption spectra of HSA with increasing concentration of **L** at 298 K in PBS buffer (pH 7.4).

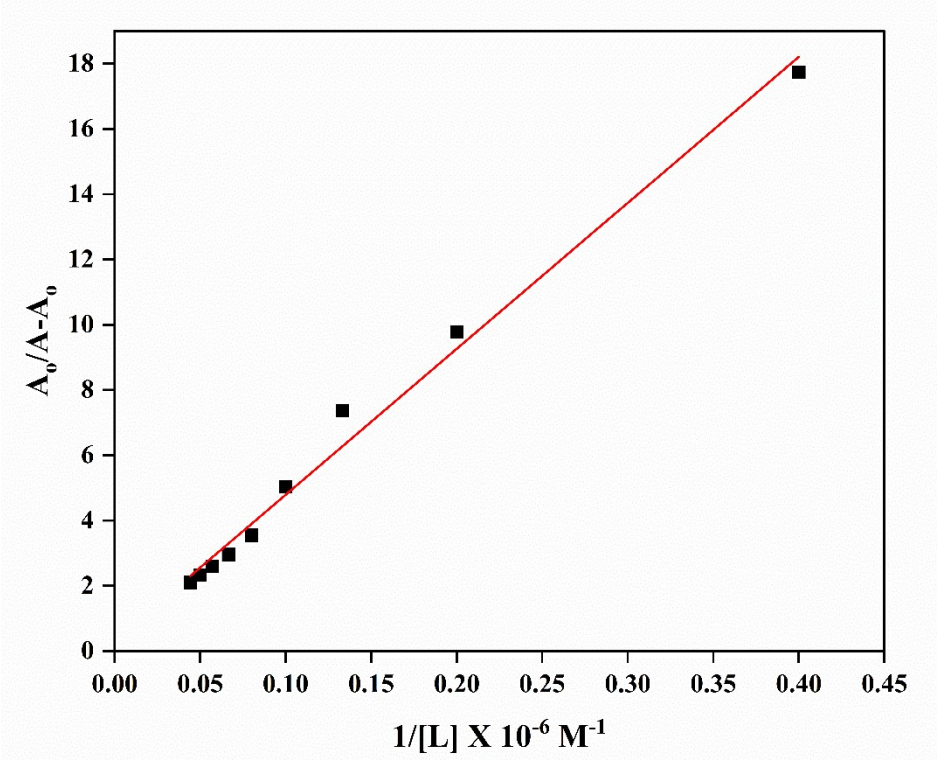

Figure S17: Benesi-Hildebrand plot $\{A_o/(A-A_o)$ vs. 1/ **[L]**$\}$ of absorption spectra of HSA in the absence and presence of **L** in PBS buffer at 298 K.

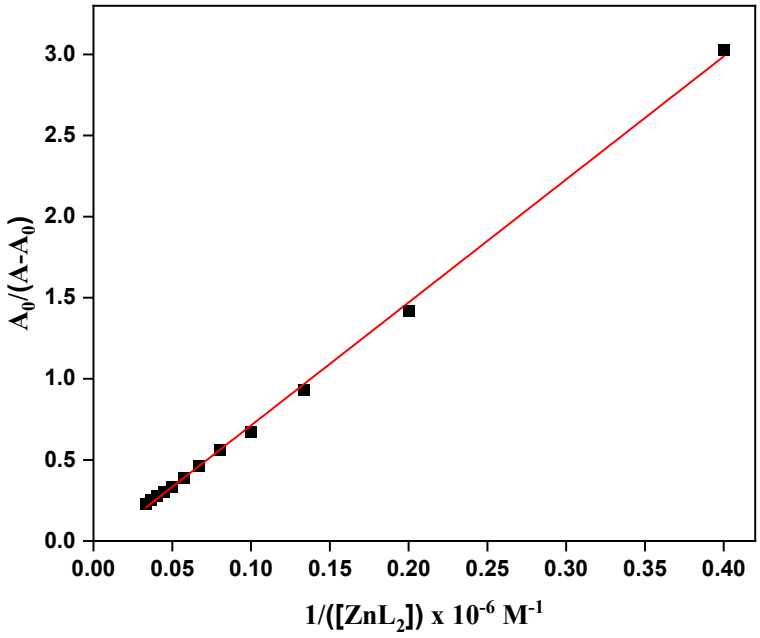

Figure S18: Benesi-Hildebrand plot $\{A_o/(A-A_o)$ vs. $1/$ **[**ZnL_2**]**$\}$ of absorption spectra of HSA in the absence and presence of ZnL_2 in PBS buffer at 298 K.

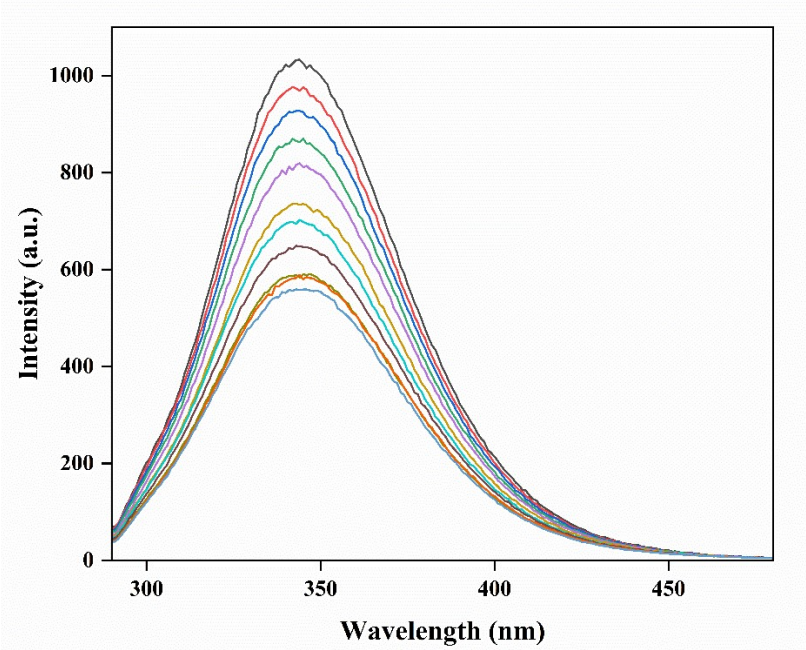

Figure S19: Emission spectra of HSA with increasing concentration of **L** at 298 K in PBS buffer (pH 7.4).

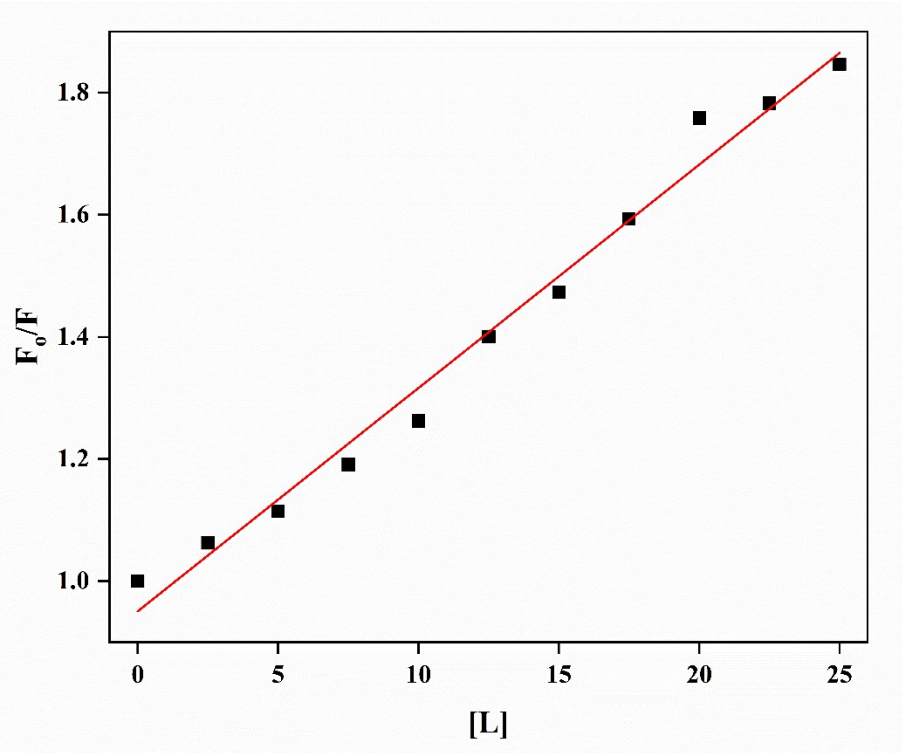

Figure S20: Stern-Volmer plot {F_0/F vs. [**L**]} of emission spectra of HSA in the absence and presence of **L** in PBS buffer at 298 K.

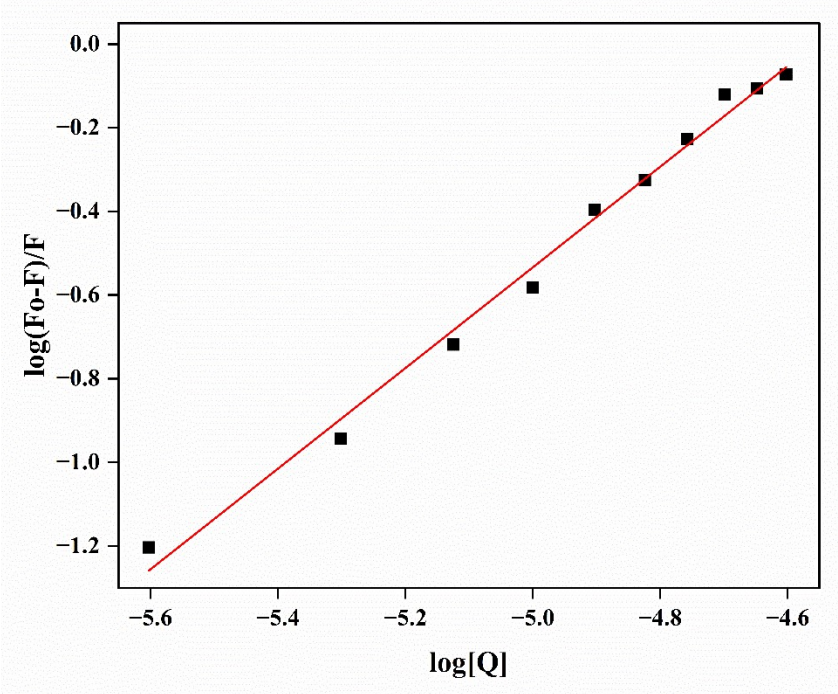

Figure S21: Modified Stern-Volmer plot of emission spectra of HSA in the absence and presence of **L** in PBS buffer at 298K

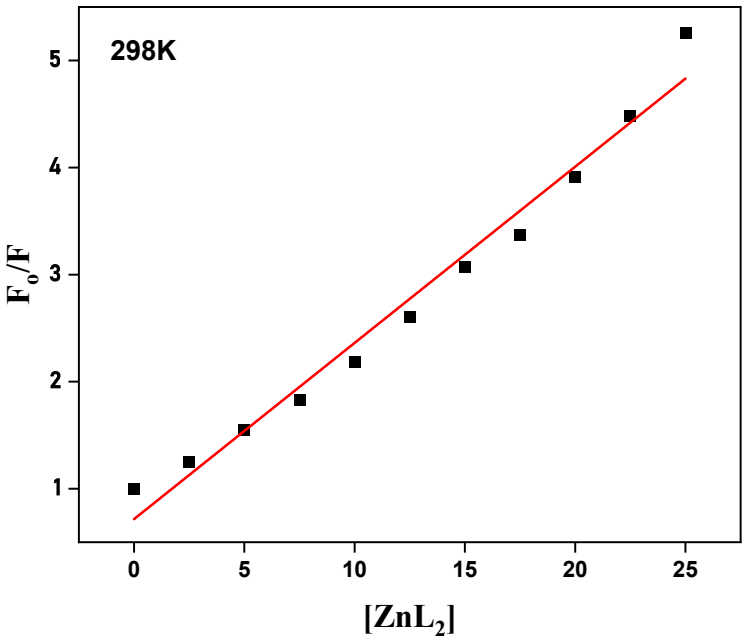

Figure S22: Stern-Volmer plot {F_0/F vs. [Zn**L**$_2$]} of emission spectra of HSA in the absence and presence of Zn**L**$_2$ in PBS buffer at 298 K.

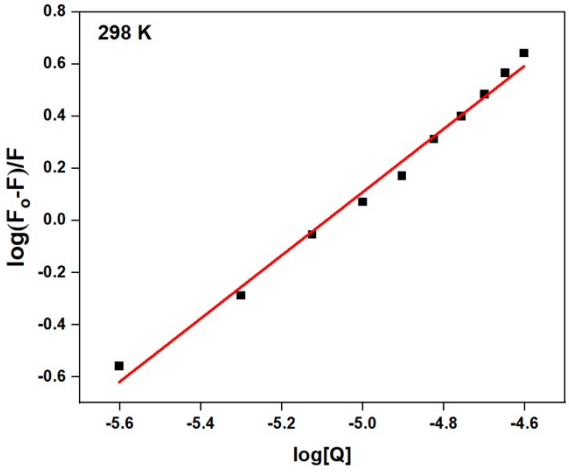

Figure S23: Modified Stern-Volmer plot of emission spectra of HSA in the absence and presence of Zn**L**$_2$ in PBS buffer at 298 K

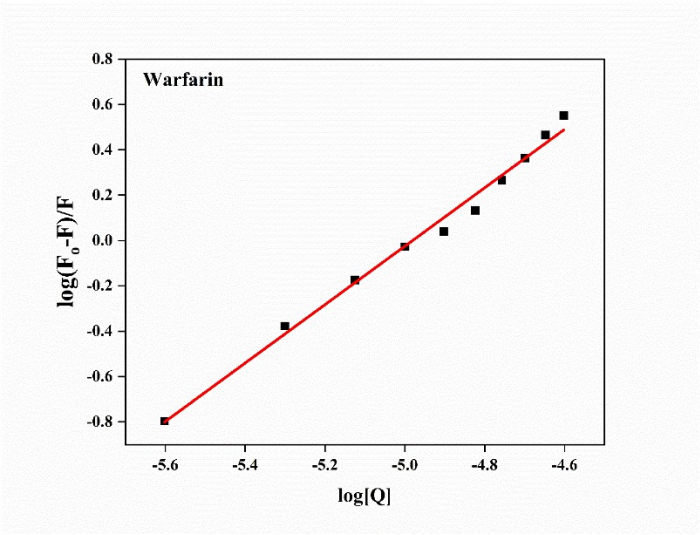

Figure S24: Modified Stern-Volmer plots of fluorescence spectrometer titration of warfarin-HSA complex with Zn$\mathbf{L_2}$

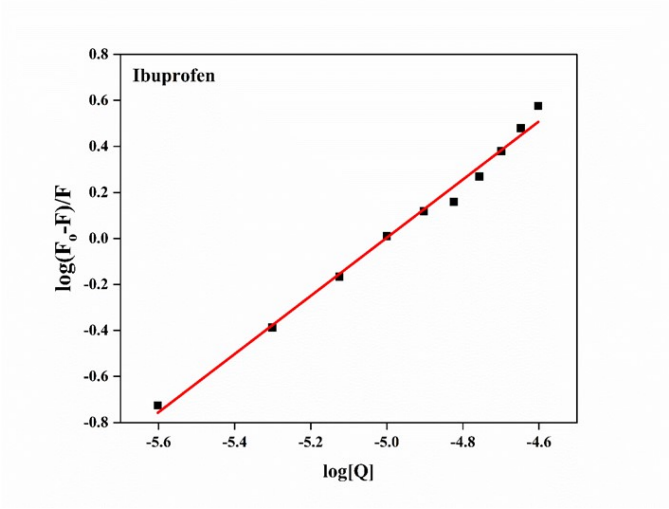

Figure S25: Modified Stern-Volmer plots of fluorescence spectrometer titration of ibuprofen-HSA complex with **Zn$\mathbf{L_2}$**

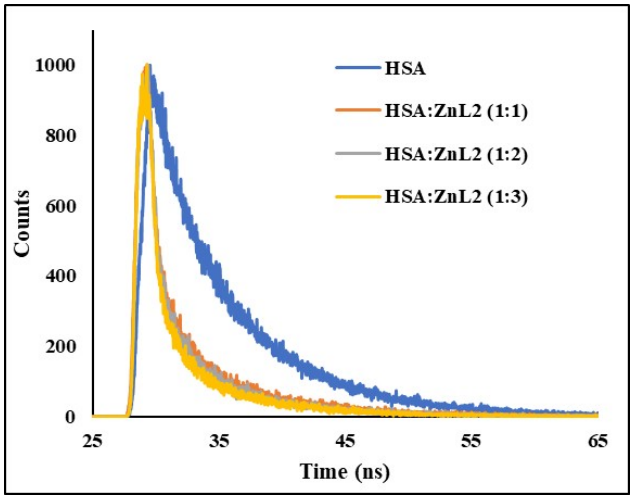

Figure S26: Time decay profile of HSA on gradual addition of Zn**L**$_2$ in PBS buffer (*p*H 7.4).

Table S4: Cartesian Coordinates of the optimized structure of ligand **L:**

Center Number	Element	Coordinates (Angstroms)		
		X	Y	Z
1	C	2.418768	-1.077476	-0.032984
2	C	1.06272	-1.371971	-0.217857
3	C	0.143187	-0.327541	-0.322105
4	C	0.607729	0.989779	-0.275043
5	C	1.980005	1.227766	-0.121587
6	N	2.836071	0.200362	0.01276
7	H	0.734572	-2.386939	-0.27389
8	H	-0.075711	1.80794	-0.359986
9	C	2.516095	2.674155	-0.108278
10	C	3.893078	2.900032	0.029199
11	C	4.377544	4.20926	0.026626
12	H	4.565871	2.075231	0.133337
13	C	2.101832	4.977885	-0.23524
14	H	5.426188	4.401418	0.126213
15	H	1.400631	5.779694	-0.334507
16	C	3.436149	-2.223414	0.122025
17	C	4.788411	-1.936853	0.36572
18	C	3.866935	-4.527573	0.158511

19	C	5.694057	-2.98726	0.517386
20	H	5.12244	-0.922198	0.436185
21	H	3.503013	-5.529809	0.070378
22	H	6.72741	-2.791271	0.712969
23	C	-1.358133	-0.625168	-0.483495
24	C	-1.796516	-1.950536	-0.60591
25	C	-2.28606	0.427221	-0.505666
26	C	-3.159912	-2.22537	-0.751275
27	H	-1.088239	-2.751701	-0.58742
28	C	-3.654553	0.153806	-0.644977
29	H	-1.95067	1.440073	-0.414411
30	C	-4.09048	-1.174151	-0.765718
31	H	-3.491167	-3.239088	-0.848921
32	N	1.665649	3.706764	-0.233468
33	N	3.016979	-3.495485	0.02582
34	C	3.469763	5.261484	-0.107505
35	C	5.227725	-4.300054	0.41134
36	H	3.814446	6.275512	-0.112772
37	H	5.901556	-5.124019	0.523151
38	O	-5.484767	-1.456079	-0.900403
39	O	-4.60802	1.224632	-0.66592
40	C	-6.044084	-1.669793	0.398282
41	H	-7.095173	-1.850043	0.309483
42	H	-5.574556	-2.515792	0.854044
43	C	-5.809651	-0.42062	1.269903
44	H	-6.225455	-0.578027	2.242811
45	H	-4.758345	-0.238654	1.357639
46	H	-6.280797	0.423773	0.813901
47	C	-5.110512	1.460389	0.654413
48	H	-5.835544	2.248077	0.621354
49	H	-5.570186	0.568227	1.025567

50	C	-3.953991	1.868043	1.588337
51	H	-3.227925	1.081812	1.622292
52	H	-3.49343	2.761766	1.221641
53	H	-4.338155	2.041871	2.571132

Table S5: Cartesian Coordinates of the optimized structure of ligand **ZnL_2:**

Center Number	Element	Coordinates (Angstroms)		
		X	Y	Z
1	C	2.686378	-1.100249	1.018253
2	C	4.070625	-1.140405	1.078139
3	C	4.855129	-0.370149	0.192982
4	C	4.157793	0.42752	-0.739728
5	C	2.772142	0.436179	-0.770561
6	H	4.557927	-1.750313	1.826067
7	H	4.714492	1.019493	-1.45285
8	C	1.98425	1.232394	-1.719178
9	C	2.537449	1.983781	-2.771555
10	C	-0.156461	1.910152	-2.343019
11	C	1.708983	2.716152	-3.602319
12	H	3.606763	1.987855	-2.937538
13	C	0.32128	2.688863	-3.383262
14	H	-1.220796	1.841177	-2.139736
15	H	2.128266	3.298625	-4.414629
16	H	-0.362575	3.252978	-4.004719
17	C	1.810375	-1.866704	1.912303
18	C	2.266063	-2.633417	2.999912
19	C	-0.388986	-2.46997	2.39212
20	C	1.359653	-3.334972	3.773858
21	H	3.321091	-2.672647	3.237395
22	C	-0.008631	-3.261526	3.462444
23	H	-1.434458	-2.365491	2.118352

24	H	1.703611	-3.928622	4.613041
25	H	-0.751238	-3.800109	4.037357
26	C	6.325255	-0.39777	0.239076
27	C	7.028117	-1.533557	0.683623
28	C	7.087858	0.717312	-0.158065
29	C	8.417549	-1.55538	0.707679
30	H	6.486347	-2.424765	0.976703
31	C	8.476983	0.704146	-0.126215
32	H	6.608085	1.637251	-0.470242
33	C	9.159974	-0.449912	0.295739
34	H	8.952297	-2.440086	1.034711
35	N	2.039427	-0.320089	0.100933
36	N	0.637055	1.200287	-1.528954
37	N	0.480657	-1.789573	1.632589
38	O	10.535241	-0.48949	0.351327
39	O	9.166184	1.822564	-0.542548
40	C	11.195242	-0.623339	-0.92569
41	H	10.869052	-1.560786	-1.39275
42	H	10.899753	0.207172	-1.574018
43	C	9.769403	2.596577	0.516433
44	H	10.454991	1.960443	1.084155
45	H	8.977441	2.943009	1.191764
46	C	10.496319	3.767589	-0.11436
47	H	9.80639	4.388283	-0.690852
48	H	10.950846	4.38715	0.663734
49	H	11.287572	3.420038	-0.782817
50	C	12.691429	-0.629157	-0.682461
51	H	13.223054	-0.747902	-1.630716
52	H	13.014504	0.307604	-0.222258
53	H	12.974304	-1.452469	-0.022366
54	Zn	-0.022562	-0.286999	0.029755
55	C	-2.760992	-1.031019	-0.942985

56	C	-2.797577	0.545838	0.810158
57	C	-4.146543	-1.023941	-1.006406
58	C	-4.183189	0.583796	0.776657
59	C	-4.904701	-0.209079	-0.140543
60	H	-4.65399	-1.63251	-1.742131
61	H	-4.721268	1.21007	1.474642
62	C	-1.909654	-1.846904	-1.817596
63	C	-2.388899	-2.618343	-2.891331
64	C	-1.505317	-3.367988	-3.646775
65	H	-3.443721	-2.623952	-3.13301
66	C	0.26821	-2.537932	-2.27504
67	C	-0.136688	-3.337621	-3.330536
68	H	-1.86716	-3.965761	-4.475443
69	H	1.315682	-2.464827	-1.998866
70	H	0.58818	-3.91457	-3.89065
71	C	-1.983888	1.33686	1.742883
72	C	-2.513477	2.127579	2.777875
73	C	-1.661613	2.850651	3.593604
74	H	-3.582099	2.169698	2.942899
75	C	0.176906	1.957767	2.353407
76	C	-0.276049	2.773966	3.376368
77	H	-2.062032	3.463535	4.392936
78	H	1.238374	1.84947	2.1526
79	H	0.425444	3.328954	3.986265
80	C	-6.375868	-0.18708	-0.190041
81	C	-7.10301	0.964516	0.167533
82	C	-7.119072	-1.307424	-0.590048
83	C	-8.488792	1.002887	0.138515
84	H	-6.594717	1.875595	0.459611
85	C	-8.511496	-1.285745	-0.622144
86	H	-6.612591	-2.230888	-0.844291
87	C	-9.219519	-0.139424	-0.255047

88	H	-9.038567	-2.184718	-0.913014
89	N	-0.579294	-1.811642	-1.533688
90	N	-2.090782	-0.253808	-0.041586
91	N	-0.639229	1.257005	1.554625
92	O	-10.5803	-0.018439	-0.250681
93	O	-9.123817	2.14732	0.555135
94	C	-9.797762	2.910869	-0.464786
95	H	-10.552709	2.286704	-0.949747
96	H	-9.060806	3.218353	-1.217649
97	C	-10.431358	4.11596	0.201785
98	H	-10.94255	4.730407	-0.544725
99	H	-11.162525	3.801083	0.949838
100	H	-9.674855	4.73027	0.695742
101	C	-11.403989	-1.164636	-0.496138
102	H	-12.376065	-0.74087	-0.754311
103	H	-11.040821	-1.710446	-1.373554
104	C	-11.52912	-2.07119	0.721837
105	H	-12.217165	-2.892849	0.501227
106	H	-10.568053	-2.499919	1.011895
107	H	-11.924445	-1.510764	1.571874

References

(S1) Das, D.; Sutradhar, S.; Singh, A.; Ghosh, B. N. Zinc-terpyridine Based Chemosensor for Detection of Pyrophosphate Anion in Aqueous Medium. *Zeitschrift für Anorg. und Allg. Chemie* **2021**, *647* (11), 1234–1238.

(S2) Zaltariov, M.-F.; Cazacu, M.; Avadanei, M.; Shova, S.; Balan, M.; Vornicu, N.; Vlad, A.; Dobrov, A.;Varganici, C.-D. Synthesis, characterization and antimicrobial activity of new Cu(II) and Zn(II) complexes with Schiff bases derived from trimethylsilyl-propyl-p-aminobenzoate. *Polyhedron* **2015**, *100*, 121–131.

(S3) Abu Ali, H.; Omar, S.N.; Darawsheh, M.D.; Fares, H. Synthesis, characterization and antimicrobial activity of zinc(II) ibuprofen complexes with nitrogen-based ligands. *J. Coord. Chem.* **2016**, *69*, 1110–1122.

(S4) Andrejević, T. P., Aleksic, I., Kljun, J., Pantović, B. V., Milivojevic, D., Vojnovic, S.,

Turel, I., Djuran, M. I., & Glišić, B. Đ. Zinc(II) Complexes with Dimethyl 2,2′-Bipyridine-4,5-dicarboxylate: Structure, Antimicrobial Activity and DNA/BSA Binding Study. *Inorganics*, **2022**, *10*(6), 71.

(S5) Jaafar, A., Fix-Tailler, A., Mansour, N., Allain, M., Shebaby, W. N., Faour, W. H., ... & Ibrahim, G. Synthesis, characterization, antifungal and antibacterial activities evaluation of copper (II), zinc (II) and cadmium (II) chloride and bromide complexes with new (E)-1-(3, 4-dimethoxybenzylidene)-4-methylthiosemicarbazone ligand. *Appl. Organomet. Chem.*, **2020**, *34(12)*, e5988.

(S6) Rashidi, N., Fard, M. J. S., Hayati, P., Janczak, J., Yazdian, F., Rouhani, S., & Msagati, T. A. Antibacterial and cytotoxicity assay of two new Zn (ii) complexes: Synthesis, characterization, X-ray structure, topology, Hirshfeld surface and thermal analysis. *J. Mol. Struct.*, **2021**, *1231*, 129947.

(S7) Bruker, A. X. S. Apex2, Saint and Sadabs. . Bruker AXS Inc. Madison, Wisconsin, USA 2009.

(S8) Sheldrick, G. M. SADABS, Version 2.10. *Univ. Göttingen, Ger.* **2003**.

(S9) Sheldrick, G. M. SHELXT–Integrated Space-Group and Crystal-Structure Determination. *Found. Crystallogr.* **2015**, *71* (1), 3–8.

(S10) Sheldrick, G. M. Crystal Structure Refinement with SHELXL. *Cryst. Struct. Commun.* **2015**, *71* (1), 3–8.

(S11) Macrae, C. F.; Bruno, I. J.; Chisholm, J. A.; Edgington, P. R.; McCabe, P.; Pidcock, E.; Rodriguez-Monge, L.; Taylor, R.; Streek, J. V. D.; Wood, P. A. Mercury CSD 2.0–New Features for the Visualization and Investigation of Crystal Structures. *J. Appl. Crystallogr.* **2008**, *41* (2), 466–470.